AMERICAN SOCIETY FOR MICROBIOLOGY | Infection and Immunity®

BACTERIAL INFECTIONS

# The PerR-Regulated $P_{1B-4}$-Type ATPase (PmtA) Acts as a Ferrous Iron Efflux Pump in *Streptococcus pyogenes*

**Andrew G. Turner,[a] Cheryl-lynn Y. Ong,[a] Karrera Y. Djoko,[a] Nicholas P. West,[a] Mark R. Davies,[a,b] Alastair G. McEwan,[a] Mark J. Walker[a]**

School of Chemistry and Molecular Biosciences and Australian Infectious Diseases Research Centre, The University of Queensland, Brisbane, QLD, Australia[a]; Department of Microbiology and Immunology, University of Melbourne, at the Peter Doherty Institute for Infection and Immunity, Melbourne, VIC, Australia[b]

**ABSTRACT** *Streptococcus pyogenes* (group A *Streptococcus* [GAS]) is an obligate human pathogen responsible for a broad spectrum of human disease. GAS has a requirement for metal homeostasis within the human host and, as such, tightly modulates metal uptake and efflux during infection. Metal acquisition systems are required to combat metal sequestration by the host, while metal efflux systems are essential to protect against metal overload poisoning. Here, we investigated the function of PmtA (PerR-regulated metal transporter A), a $P_{1B-4}$-type ATPase efflux pump, in invasive GAS M1T1 strain 5448. We reveal that PmtA functions as a ferrous iron [Fe(II)] efflux system. In the presence of high Fe(II) concentrations, the 5448Δ*pmtA* deletion mutant exhibited diminished growth and accumulated 5-fold-higher levels of intracellular Fe(II) than did the wild type and the complemented mutant. The 5448Δ*pmtA* deletion mutant also showed enhanced susceptibility to killing by the Fe-dependent antibiotic streptonigrin as well as increased sensitivity to hydrogen peroxide and superoxide. We suggest that the PerR-mediated control of Fe(II) efflux by PmtA is important for bacterial defense against oxidative stress. PmtA represents an exemplar for an Fe(II) efflux system in a host-adapted Gram-positive bacterial pathogen.

**KEYWORDS** iron efflux, PmtA, oxidative stress response, PerR, group A *Streptococcus*, *Streptococcus pyogenes*

**Received** 22 February 2017 **Returned for modification** 20 March 2017 **Accepted** 25 March 2017

**Accepted manuscript posted online** 3 April 2017

**Citation** Turner AG, Ong CY, Djoko KY, West NP, Davies MR, McEwan AG, Walker MJ. 2017. The PerR-regulated $P_{1B-4}$-type ATPase (PmtA) acts as a ferrous iron efflux pump in *Streptococcus pyogenes*. Infect Immun 85:e00140-17. https://doi.org/10.1128/IAI.00140-17.

**Editor** Nancy E. Freitag, University of Illinois at Chicago



Address correspondence to Mark J. Walker, mark.walker@uq.edu.au.

A.G.M. and M.J.W. contributed equally to this work.

Defense against peroxide is recognized as one of the most widespread stress responses in prokaryotes. A characteristic of the peroxide stress response is the increased expression of peroxidases that can directly remove hydrogen peroxide as well as the induction of systems that can repair damaged proteins and nucleic acids (1, 2). *Streptococcus pyogenes* (group A *Streptococcus* [GAS]) coordinates oxidative stress responses through the action of the regulator PerR, which functions as a repressor of oxidative stress defense genes under normal conditions through binding to DNA at *per* boxes upstream of these genes (3, 4). This stable complex typically exists with Fe as a prosthetic group; in the presence of hydrogen peroxide, Fe causes metal-catalyzed oxidation and damage of the complex, leading to its dissociation and the subsequent transcription of peroxide response genes (3–6). In GAS, the PerR-regulated oxidative stress response encompasses both direct mechanisms, involving the detoxification of reactive oxygen species (ROS), and indirect mechanisms, which involve the repair of biomolecules damaged by oxidative stress. Direct mechanisms involving the enzymatic detoxification of reactive oxygen species are achieved through alkyl hydroperoxidases and glutathione peroxidases (1, 2, 5) as well as a single superoxide dismutase, SodA, which is Mn dependent (7). An example of an indirect response mechanism is PolAI, a DNA polymerase that repairs oxidatively damaged DNA (8).

Another strategy employed by bacteria to ameliorate the effects of peroxide stress is to control the intracellular concentration of prooxidant metal ions so as to minimize the Fenton reaction (10, 11). Cu(I) and Fe(II) are biologically available metal elements capable of potentiating Fenton chemistry. In the case of Fe(II), one aspect of the bacterial peroxide stress response involves the decreased expression of Fe uptake systems and the increased expression of Fe storage proteins that effectively sequester Fe and thus prevent prooxidant activity (12–14). In contrast, copper concentrations within the bacterial cell are held very low as a consequence of the action of a Cu efflux system (CopYAZ) that is controlled by a Cu-sensing regulator (CopY) (15–17). The possibility that Fe ions might also be effluxed from the bacterial cell during peroxide stress has not been widely investigated. Recently, however, two P-type ATPases that mediate bacterial Fe efflux, PfeT of *Bacillus subtilis*, which is regulated by Fur and PerR (18), and FrvA of *Listeria monocytogenes*, which is regulated by Fur (19), have been described.

GAS is an obligate human pathogen responsible for approximately 600,000 deaths annually (20). Disease states range from mild infections of the skin (impetigo) and pharynx ("strep throat") to severe invasive disease such as necrotizing fasciitis and streptococcal toxic shock syndrome. Repeated infection can also lead to postinfectious immune sequelae such as poststreptococcal glomerulonephritis and rheumatic heart disease (21). As a host-adapted human pathogen, GAS deploys multiple systems for resisting innate and adaptive immunity during colonization and infection (21, 22). These systems include mechanisms for defense against oxidative stress (23). To date, the capacity of GAS to efflux Fe as part of the oxidative stress response has not been investigated.

In this work, we describe the role of the cation transport protein denoted PmtA (PerR-regulated metal transporter A) (SPy1167), a P-type ATPase, as a PerR-regulated efflux protein of GAS with specificity for Fe(II). Additionally, we demonstrate that Fe(II) efflux provides increased resistance to oxidative stress through the efflux of prooxidant Fe(II) under conditions of oxidative stress.

## RESULTS

**PmtA is a $P_{1B-4}$-type ATPase.** PmtA (SPy1167) is annotated in the M1T1 reference genome (MGAS5005) (24) as a P-type ATPase (25). However, there are multiple subclasses of class $P_{1B}$-type ATPases in bacteria, each with various metal specificities. Metal ion specificity has previously been shown to depend on specific amino acid sequences within transmembrane (TM) regions of the protein (26). In order to classify PmtA within P-type ATPase class designations, an amino acid alignment of GAS PmtA with other annotated $P_{1B-4}$-type ATPases from different bacteria (NCBI nonredundant GenBank database) was performed using MUSCLE (27). Following amino acid alignment and hydrophobicity analysis using TMHMM (28), the transmembrane region was analyzed in order to determine the $P_{1B}$ subclass (29, 30). $P_{1B-4}$ ATPases feature a characteristic SPC amino acid metal binding motif in transmembrane region 4 and an HEG(G/S)T metal binding motif in transmembrane region 6 (29). This analysis confirmed that PmtA is a $P_{1B-4}$ P-type ATPase, a classification identical to that of PfeT and FrvA (Fig. 1A; see also Fig. S1 in the supplemental material for the full alignment).

Phylogenetic analysis indicates that GAS PmtA is closely related to the $P_{1B-4}$-type ATPases from other lactic acid bacteria (clade a) (Fig. 1B). Within this clade, the $P_{1B-4}$-type ATPase lineage is differentiated into two clusters. GAS PmtA is closely related to PmtA homologs found in other genetically related streptococcal species, including *S. dysgalactiae* and *S. canis*, and a *Chlamydia trachomatis* PmtA homolog, which share >90% amino acid identity (Fig. 1B, yellow shading, and Fig. S1). Furthermore, *S. pyogenes* PmtA is genetically distinct from the lineages made up of functionally characterized $P_{1B-4}$-type ATPase family members *B. subtilis* PfeT (43% identity) (clade b) and *L. monocytogenes* FrvA (47% identity) (clade e) (Fig. 1B).

**A 5448Δ*pmtA* mutant is sensitive to high extracellular Fe(II) concentrations.** To investigate the role of *pmtA* in GAS physiology, we created an isogenic gene deletion

A

| | | Transmembrane 4 | Transmembrane 6 |
|---|---|---|---|
| *Streptococcus pyogenes* PmtA | 100% | LLTVASPCALIASSTPASLAAIS | LPLGVVGHEGSTILVILNGLRLL |
| *Streptococcus dysgalactiae* | 94.9% | LLTVASPCALIASSTPASLAAIS | LPLGVVGHEGSTILVILNGLRLL |
| *Streptococcus canis* | 92.1% | LLTVASPCALIASSTPASLSAIS | LPLGVVGHEGSTILVILNGLRLL |
| *Chlamydia trachomatis* | 90.1% | LLTVASPCALIASSTPASLSAIS | LPLGVVGHEGSTILVILNSLRLL |
| *Streptococcus iniae* | 73.6% | LLTVASPCALVAASTPASLSAIS | LPLGVVGHEGSTILVILNGLRLL |
| *Streptococcus porcinus* | 73.5% | LLTVASPCALIASSTPASLSAIS | LPLGVVGHEGSTILVILNGLRLL |
| *Streptococcus suis* | 59.8% | LLTIASPCALVASSSPATLSAIS | LPLGVVGHEGSTILVILNGLRLL |
| *Listeria monocytogenes* FrvA | 47.1% | LLTVASPCALVASVTPATLAAIS | LPFGVVGHEGSTILVILNGLRLL |
| *Enterococcus faecium* | 45.2% | LIVVASPCALVASATPATLAALS | LPFGVIGHEGSTILVILNGLRLL |
| *Streptococcus pneumoniae* | 44.8% | FMVVASPCALVASIMPAALSLIS | LPFGVIGHEGSTILVILNGLRLL |
| *Enterococcus faecalis* | 44.9% | LLVVASPCALVASATPATLAALS | LPIGVVGHEGSTILVILNGLRLL |
| *Bacillus subtilis* PfeT | 42.8% | LLVVASPCALVAAITPATLSAIS | LPFGVIGHEGSTILVILNGLRLL |
| *Streptococcus thermophilus* | 38.7% | YLIGVSPCALAASAVPATLAAMS | IGWGVVLHEGSTILVLLNGLRLL |
| *Streptococcus mutans* | 37.7% | FLVSASPCALAVSVIPATLAGIS | VVASVALHEGSTLIVLLNSLRLL |
| *Cupriavidus metallidurans* CzcP | 35.1% | VLVAASPCALAIATPSAVLSGVA | IGPAVAMHEGSTLIVVFNALRLL |
| *Streptococcus agalactiae* | 36.0% | FLIAASPCALAASAVPATLSGIS | IAFSVLIHEGSTLVVIFNGLRLL |
| *Sulfitobacter* sp. NAS14.1 sCoatT | 32.7% | VLVAASPCALAIATPSAVLSGVA | IGPAVLVHEGSTLVVVANALRLL |
| *Mycobacterium tuberculosis* CtpD | 32.7% | FMIVASPCAVVLATMPPLLSAIA | LPLGVVGHEGSTVLVALNGMRLL |
| *Mycobacterium smegmatis* CtpD | 33.0% | FMIVASPCAVVLATMPPLLSAIA | LPLGVAGHEGSTILVALNGLRLL |
| *Mycobacterium tuberculosis* CtpJ | 32.7% | FMIVASPCAVVLATMPPLLAAIA | LPLGVARHEGSTIIVGLNGLRLL |
| consensus (100%) | | hhh.sSPCAlhhu..ss.Luhhu | ls.uVhhHEGSTllVhhNuhRLL |

B

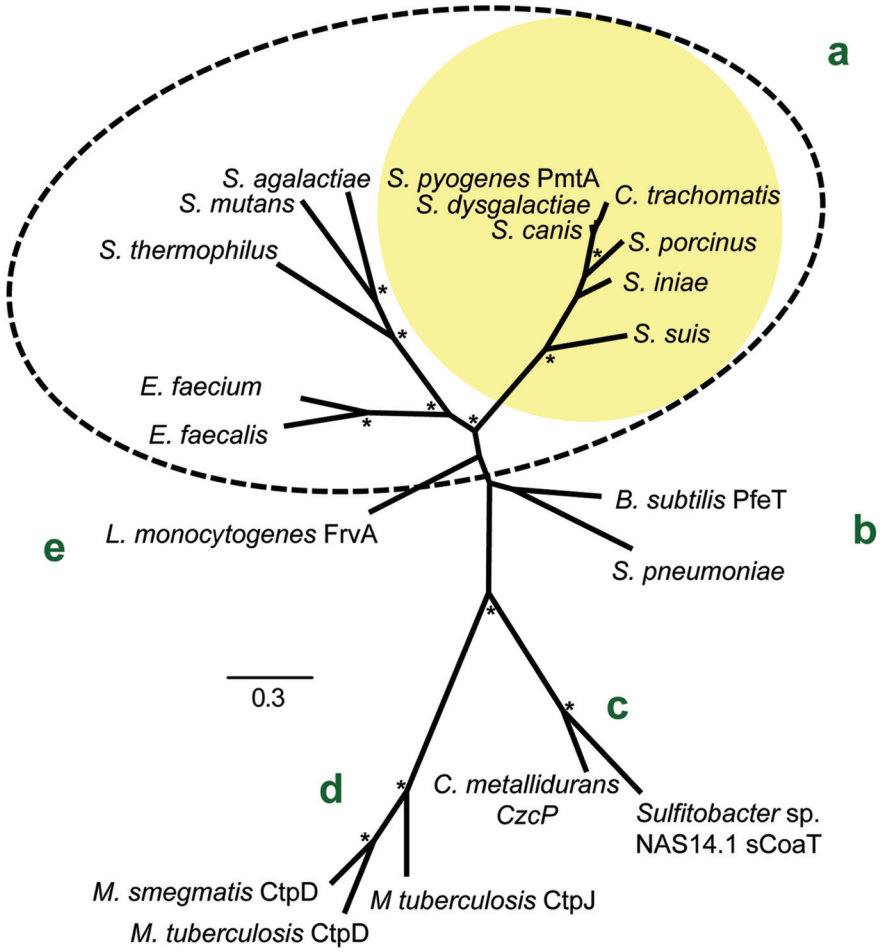


**FIG 1** Phylogenetic clustering and high-level conservation of key motifs within transmembrane helices of *S. pyogenes* PmtA and homologous $P_{1B-4}$-type ATPase family transporters. Amino acid sequences of $P_{1B-4}$-type ATPases from 20 bacterial species with close homology to GAS PmtA as well as previously characterized $P_{1B-4}$-type ATPases were used for analysis. (A) Multiple-sequence alignment of TM helices 4 and 6 from the PmtA and $P_{1B-4}$-type ATPase family protein alignment (see Fig. S1 in the supplemental material). Key conserved motifs within TM helices 4 and 6 are highlighted in blue, and the essential serine residue within TM helix 6 is highlighted in red. Consensus patterns based on discriminating equivalence class at a 100% threshold are indicated below the alignment. Percent amino acid identities relative to *S. pyogenes* PmtA (TM helices 1 to 6) are indicated next to the species name. (B) Unrooted maximum-likelihood phylogenetic tree of *S. pyogenes* PmtA-related sequences based on protein sequences derived from the six core transmembrane helices common to the $P_{1B-4}$-type ATPase family. The corresponding multiple-sequence alignment is presented in Fig. S1 in the supplemental material. The bar indicates the number of amino acid

(Continued on next page)

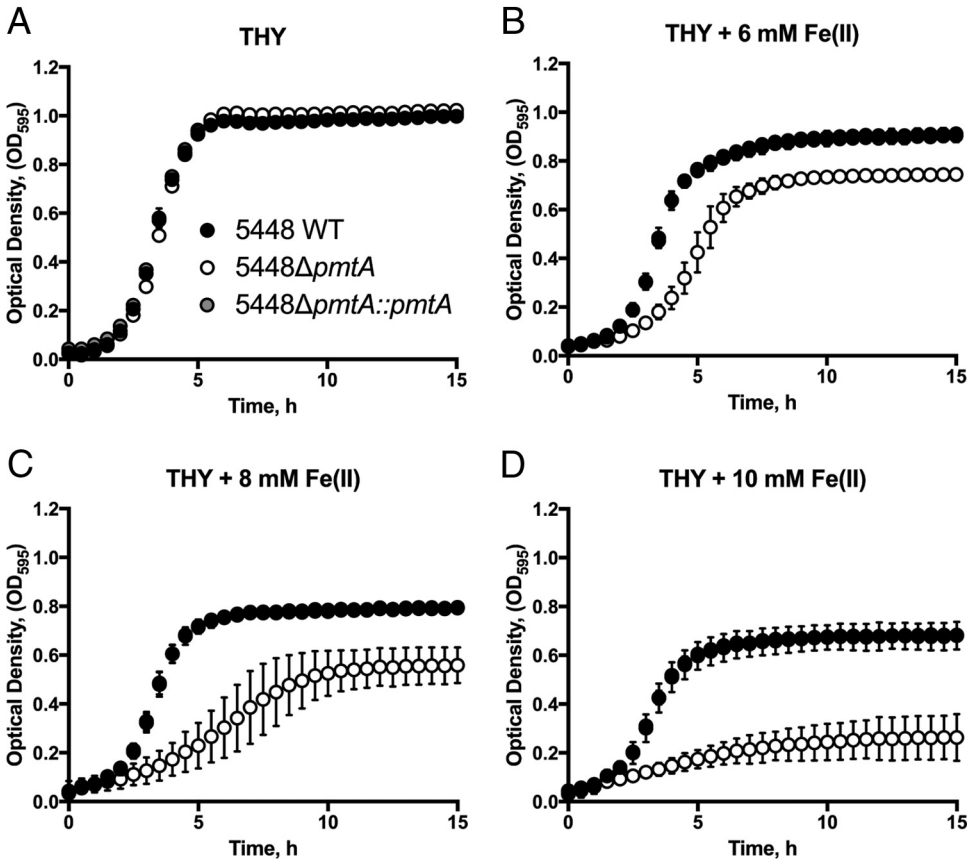


**FIG 2** Growth curve analysis in the presence of Fe(II). Cultures of strains 5448 WT, 5448Δ*pmtA*, and 5448Δ*pmtA*::*pmtA* grown overnight were diluted to a starting $OD_{600}$ of 0.05 in THY broth (A) or THY broth supplemented with 6 mM (B), 8 mM (C), or 10 mM (D) Fe(II). Growth at 37°C was monitored by recording the $OD_{595}$. Graphs represent means ± standard deviations of data from 3 independent biological replicates.

mutant in invasive GAS M1T1 isolate 5448 (31). Briefly, the 5448Δ*pmtA* strain was constructed by allelic exchange of the *ahpA3* cassette with *pmtA* (*SPy1167*). The 5448Δ*pmtA* mutant was complemented through the exchange of *ahpA3* with the wild-type (WT) *pmtA* allele. We examined the growth characteristics of wild-type strain 5448 (5448 WT), 5448Δ*pmtA*, and 5448Δ*pmtA*::*pmtA* with various metal concentrations. In Todd-Hewitt broth supplemented with 1% (wt/vol) yeast extract (THY broth) alone, all strains grew equivalently (Fig. 2A). However, in the presence of 8 mM Fe(II), 5448Δ*pmtA* exhibited a prolonged doubling time (3.4 ± 0.2 h [standard deviation {SD}] versus 1.3 ± 0.2 h [SD] for the WT and 1.4 ± 0.1 h [SD] for 5448Δ*pmtA*::*pmtA*; $P < 0.0001$) and reached a lower final cell yield than did 5448 WT and 5448Δ*pmtA*::*pmtA* with identical treatments (Fig. 2C). This reduction in the growth rate and endpoint density in the 5448Δ*pmtA* mutant became more pronounced with increasing concentrations of Fe(II) (Fig. 2B to D). A similar effect was noted with Co(II), where 5448Δ*pmtA* showed a diminished growth rate and reached a lower stationary-phase optical density (OD) than did 5448 WT and 5448Δ*pmtA*::*pmtA* under the same conditions (see Fig. S2 in the supplemental material). This growth defect of the 5448Δ*pmtA* mutant was restored in the complemented mutant. Growth analysis in the presence of Mn(II), Ni(II), Cu(II), or Zn(II) showed no difference in the growth of the 5448Δ*pmtA* mutant relative to 5448 WT or 5448Δ*pmtA*::*pmtA* (Fig. S3 to S6).

**FIG 1** Legend (Continued)
substitutions per site under the WAG substitution model. Asterisks indicate bootstrap values greater than 90 (out of 100 replicates). The dashed oval denotes clade a, and yellow shading highlights subclade a containing PmtA of GAS.

**Intracellular metal accumulation by 5448Δ*pmtA*.** Based on the finding that 5448Δ*pmtA* is sensitive to high concentrations of Fe(II), we sought to determine whether this sensitivity arose through an inability to efflux this metal ion. Inductively coupled plasma mass spectrometry (ICP-MS) was used to analyze the intracellular metal accumulation of 5448 WT, 5448Δ*pmtA*, and 5448Δ*pmtA*::*pmtA* grown in THY broth after challenge with Fe(II). In the absence of additional Fe(II) in the medium, 5448Δ*pmtA* accumulated approximately 2-fold-higher levels of intracellular Fe than did 5448 WT and the complemented mutant (Fig. 3A) ($P < 0.001$). Intracellular Fe accumulation was increased in all strains following the addition of 8 mM Fe(II). However, the 5448Δ*pmtA* mutant accumulated approximately 5-fold more Fe than did 5448 WT and the complemented mutant (Fig. 3B) ($P < 0.0001$). ICP-MS was also used to analyze intracellular metal accumulation after the addition of Co(II) and Zn(II). Only Co significantly accumulated in the 5448Δ*pmtA* background (see Fig. S7 in the supplemental material). In addition to the lack of growth inhibition of the 5448Δ*pmtA* mutant by Zn(II) (Fig. S6), the lack of significantly higher Zn accumulation in the 5448Δ*pmtA* strain when challenged by Zn(II) suggests that PmtA does not function as a Zn exporter, as previously hypothesized (25).

**Streptonigrin exerts a toxic effect against 5448Δ*pmtA*.** Based on the observation of increased intracellular Fe levels within the 5448Δ*pmtA* mutant, we hypothesized that this mutant would show greater susceptibility to streptonigrin. Streptonigrin is an aminoquinone antibiotic that exerts Fe-dependent toxicity against bacteria (32). The addition of 200 nM streptonigrin to THY broth resulted in an increased doubling time (2.4 ± 0.3 h [SD] versus 1.3 ± 0.2 h [SD] for the WT and 1.4 ± 0.4 h [SD] for 5448Δ*pmtA*::*pmtA*; $P < 0.01$) and a reduced stationary-phase optical density of the 5448Δ*pmtA* mutant (Fig. 3D and E). Furthermore, 250 nM streptonigrin completely inhibited the growth of the 5448Δ*pmtA* mutant compared to 5448 WT and the complemented mutant, which grew normally (Fig. 3F). This result further supports the view that PmtA is involved in Fe efflux and that elevated intracellular Fe levels in the 5448Δ*pmtA* mutant (due to the inability to efflux the metal) result in toxicity to the cell.

**Changes in *pmtA* gene expression profiles under different conditions.** Given that the 5448Δ*pmtA* mutant was found to be sensitive to Fe(II), we sought to assess the nature of *pmtA* regulation. Thus, 5448 WT was grown in the presence of subinhibitory concentrations of Fe(II) and the Fe chelator 2,2′-dipyridyl, and the gene expression of *pmtA* was examined by reverse transcriptase quantitative real-time PCR (RT-qPCR). Consistent with data from our growth analysis, we observed a 4-fold upregulation of *pmtA* in the presence of Fe(II) (Fig. 4A), while the addition of the Fe chelator 2,2′-dipyridyl resulted in an approximately 16-fold downregulation of *pmtA* (Fig. 4A).

A consensus *per* box, the regulatory element bound by PerR, is found immediately upstream of the *pmtA* gene (6, 25, 33). We therefore sought to determine whether *pmtA* is upregulated by hydrogen peroxide, consistent with PerR regulation. Quantitative gene expression data for 5448 WT indicated that *pmtA* is upregulated approximately 4-fold when exposed to 5 mM $H_2O_2$ and approximately 8-fold when exposed to 8 mM Fe(II) (Fig. 4B). This upregulation was PerR dependent, as *pmtA* gene expression was constitutive in 5448Δ*perR*. Gene regulation was restored to wild-type levels in the 5448Δ*perR* complemented mutant, suggesting that hydrogen peroxide and Fe(II) induce *pmtA* in a PerR-dependent manner.

**Growth of 5448Δ*pmtA* is inhibited by reactive oxygen species.** As excess intracellular Fe is capable of potentiating oxidative stress in biological systems, we hypothesized that Fe accumulation in the 5448Δ*pmtA* mutant may result in increased susceptibility to oxidative stress. Thus, growth analysis of strains 5448 WT, 5448Δ*pmtA*, and 5448Δ*pmtA*::*pmtA* was performed in the presence of hydrogen peroxide. In the presence of up to 3 mM hydrogen peroxide alone, the 5448Δ*pmtA* mutant grew at a rate equivalent to those of 5448 WT and the complemented mutant (see Fig. S8 in the supplemental material). However, when cells were pretreated with a subinhibitory

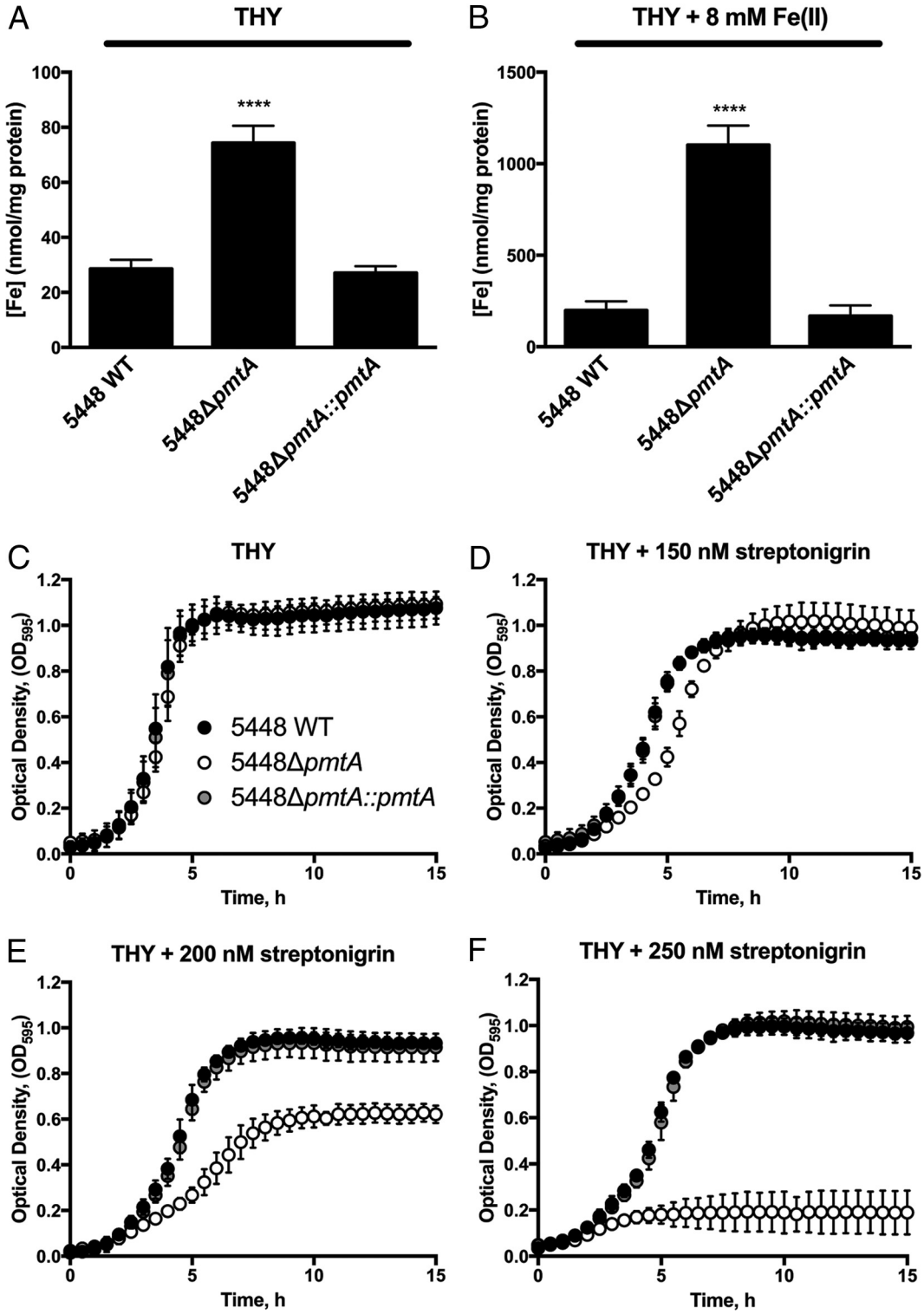


**FIG 3** Intracellular Fe accumulation and streptonigrin sensitivity. (A and B) Mid-exponential-growth-phase cultures ($OD_{600}$ = 0.6 to 0.8) of strains were challenged with sterile water (A) or 8 mM Fe(II) (B). Cells were analyzed by ICP-MS, with metal accumulation normalized to the total protein content. Graphs represent means and standard deviations of data from 3 independent experiments (1-way ANOVA was used for all comparisons to 5448 WT under each condition [**, $P < 0.01$; ***, $P < 0.001$; ****, $P < 0.0001$]). (C to F) Growth curve analysis of strains 5448 WT, 5448Δ*pmtA*, and 5448Δ*pmtA*::*pmtA*. Cultures grown overnight were diluted to an $OD_{600}$ of 0.05 in THY broth alone (C) or THY broth with 150 nM (D), 200 nM (E), or 250 nM (F) streptonigrin. Growth at 37°C was monitored by recording the $OD_{595}$. Graphs represent means ± standard deviations of data from 3 independent biological replicates.

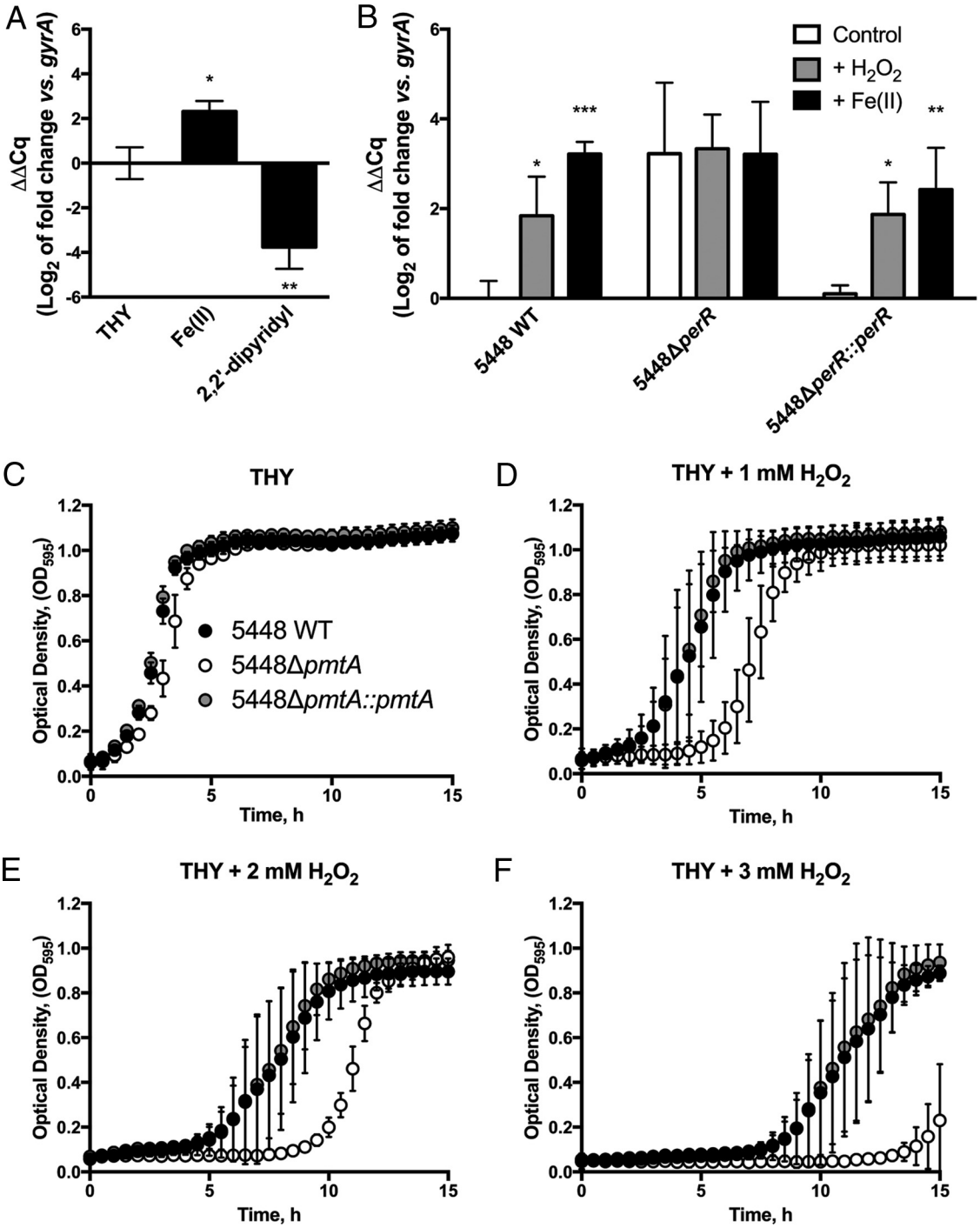


**FIG 4** Gene expression analysis of *pmtA* and $H_2O_2$ stress sensitivity. (A) 5448 WT was grown in the presence of Fe(II) or 2,2′-dipyridyl, and gene expression of *pmtA* was analyzed. (B) 5448 WT, 5448Δ*perR*, and 5448Δ*perR*::*perR* cells grown at 37°C to mid-exponential phase ($OD_{600}$ = 0.6 to 0.8) were challenged with water (control), 5 mM $H_2O_2$, or 8 mM Fe(II) for 30 min. *pmtA* gene expression was analyzed by qPCR using *gyrA* as the reference gene. Data represent the mean $\Delta\Delta C_q$ ($\log_2$) values ± standard deviations from 3 independent biological replicates (2-way ANOVA was used for all comparisons to the control for each strain [*, $P < 0.05$; **, $P < 0.01$; ***, $P < 0.001$]). (C to F) Growth curve analysis of 5448 WT, 5448Δ*pmtA*, and 5448Δ*pmtA*::*pmtA* in hydrogen peroxide. Strains were grown in THY broth plus 2 mM Fe(II) to mid-exponential phase (OD = 0.6 to 0.8) and diluted to an $OD_{600}$ of 0.05 in THY broth with 0.00 mM (C), 1 mM (D), 2 mM (E), or 3 mM (F) $H_2O_2$. Growth at 37°C was monitored by recording the $OD_{595}$. Graphs represent means ± standard deviations of data from 3 independent biological replicates.

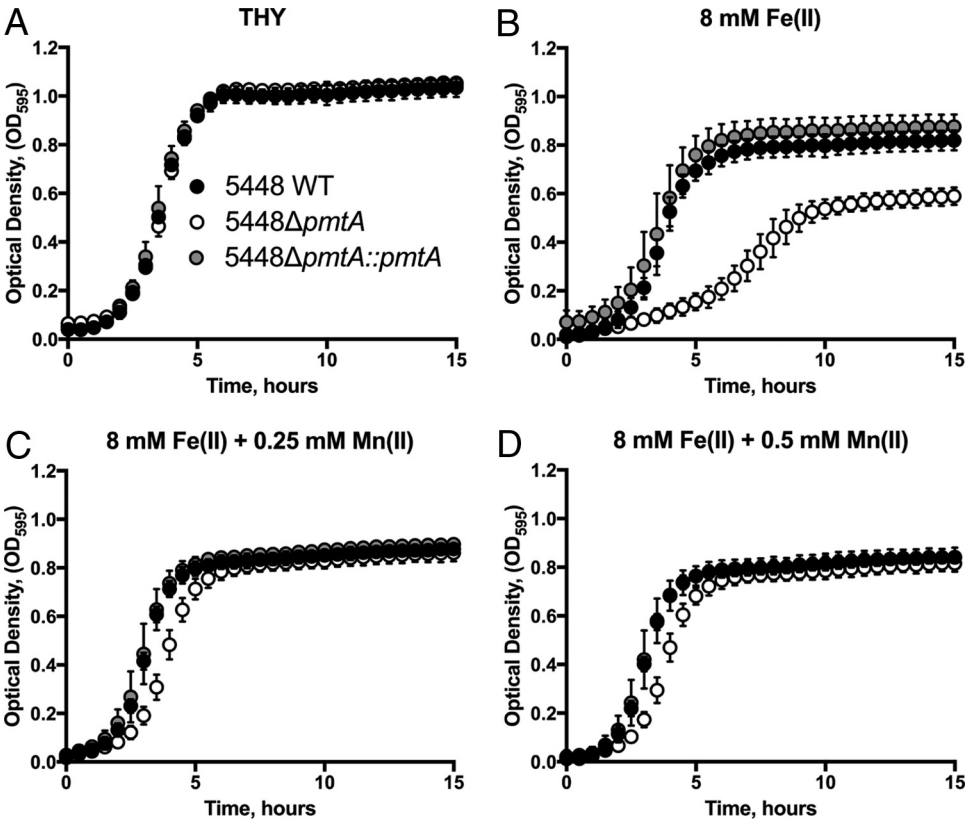


**FIG 5** Growth curve analysis of 5448 WT, 5448Δ*pmtA*, and 5448Δ*pmtA*::*pmtA* in Fe(II) and rescue of the 5448Δ*pmtA* mutant by Mn(II). Cultures of strains 5448 WT, 5448Δ*pmtA*, and 5448Δ*pmtA*::*pmtA* grown overnight were diluted to an $OD_{600}$ of 0.05 in THY broth (A) or THY broth with 8 mM Fe(II) (B), 8 mM Fe(II) plus 0.25 mM Mn(II) (C), or 8 mM Fe(II) plus 0.5 mM Mn(II) (D). Growth at 37°C was monitored by recording the $OD_{595}$. Graphs represent means ± standard deviations of data from 3 independent biological replicates.

concentration of Fe(II) (2 mM), the 5448Δ*pmtA* mutant exhibited a prolonged lag phase and impaired growth in the presence of increasing $H_2O_2$ concentrations (Fig. 4D to F). These data suggest that PmtA plays a role in the GAS response to hydrogen peroxide stress through the efflux of intracellular Fe(II). We additionally examined the sensitivity of the 5448Δ*pmtA* mutant using the superoxide generator methyl viologen (paraquat). In contrast to its growth in THY broth (Fig. S9A), the 5448Δ*pmtA* mutant showed an increased doubling time relative to those of 5448 WT and the complemented mutant with 1 mM paraquat (4.1 ± 0.8 h [SD] versus 2.5 ± 0.3 h [SD] for the WT and 2.5 ± 0.6 h [SD] for 5448Δ*pmtA*::*pmtA*; $P < 0.01$) and 1.25 mM paraquat (Fig. S9B and S9C). In a humanized plasminogen mouse model of invasive disease, the 5448Δ*pmtA* mutant was equally as virulent as 5448 WT and the complemented mutant (Fig. S10).

**Growth of 5448Δ*pmtA* in Fe(II) can be restored by Mn(II) supplementation.** Based on previously reported findings that the growth of a *B. subtilis pfeT* mutant in Fe(II) could be restored by the addition of Mn(II) (18), we sought to determine if Fe(II) toxicity in the 5448Δ*pmtA* mutant could be ameliorated by the addition of Mn(II). Growth of the 5448Δ*pmtA* mutant was inhibited by 8 mM Fe(II); however, growth could be restored to near-wild-type levels by the addition of 0.25 mM Mn(II) (Fig. 5). These data confirm that, similar to a *B. subtilis pfeT* mutant, Fe(II)-mediated toxicity in the 5448Δ*pmtA* mutant could be abrogated by the addition of Mn(II). Similarly, the growth defect of the 5448Δ*pmtA* mutant with 250 nM streptonigrin could also be restored by the addition of 0.25 mM Mn(II) (see Fig. S11 in the supplemental material). The ability of Mn(II) to restore the growth of the 5448Δ*pmtA* mutant was also observed for Co(II) toxicity (Fig. S12).

## DISCUSSION

During infection, GAS encounters reactive oxygen species. GAS encodes the regulator PerR, which acts to sense and coordinate the bacterial response to oxidative stress. Previous research examining the PerR regulon has shown that this regulator controls the direct detoxification of reactive oxygen species, mechanisms to repair ROS-mediated damage, and a number of genes involved in metal homeostasis (6, 33, 34). Here, we provided evidence to suggest that the PerR-regulated GAS gene *pmtA* encodes an Fe(II) efflux pump that contributes to defense against reactive oxygen species.

The acquisition of transition metal ions, such as Zn, Fe, and Mn, has emerged as an important factor in bacterial pathogenesis. Although bacterial pathogens are starved for Fe by the human host, they produce a variety of high-affinity uptake systems that can acquire this metal ion (35). Fe uptake is important for GAS pathogenesis (36); the bacterium can acquire Fe from hemoglobin (37) but not transferrin or lactoferrin (38). GAS utilizes the ABC transporters Siu and Sia in conjunction with Shr and Shp for heme uptake (36, 39, 40). Given the importance of Fe as a difficult nutrient to acquire, it had previously been assumed that Fe export is not required, but instead, excess Fe would be sequestered in ferritin or ferritin-like proteins (41), and the import of Fe would be downregulated (42). Here, we demonstrate that PmtA is a PerR-regulated GAS $P_{1B-4}$ P-type ATPase that contributes to resistance to oxidative stress through the removal of prooxidant Fe(II) from the intracellular environment. Our observations coincide with the $P_{1B-4}$ P-type ATPases PfeT of *B. subtilis* (18) and FrvA of *L. monocytogenes* (19), both of which are also Fe(II) efflux pumps regulated by the Fur family of regulators. The likely role of PmtA as an Fe(II) exporter is further supported by the observation that the *pmtA* deletion mutant accumulated higher levels of Fe(II) than did the WT strain under both normal and Fe(II) stress conditions.

The first described bacterial Fe efflux system was the cation diffusion facilitator FieF of *Cupriavidus metallidurans*, which provided resistance to high-Fe(II) stress and also had metal specificities for Cd(II), Co(II), Ni(II), and Zn(II) (43). GAS PmtA also demonstrated specificity for Co(II). While we observed that PmtA is able to efflux Fe(II) from GAS, it can also efflux Co(II), which is consistent with the function of $P_{1B-4}$-type ATPases (18, 29). PmtA was previously described to be involved in Zn(II) transport (25). Those authors' conclusions were based on microarray data demonstrating that PerR differentially regulated *pmtA* alongside genes involved in Zn transport. Furthermore, those authors reported that PmtA had high homology to ZosA of *B. subtilis* [before this protein was redefined as the Fe(II)-transporting $P_{1B-4}$-type ATPase PfeT] and that growth of the *pmtA perR* double mutant restored the Zn(II) hyperresistance phenotype observed in the *perR* mutant to near-WT levels (25). However, the accumulation of Zn in the *pmtA* mutant was not demonstrated. Here, we have shown that Zn does not accumulate in the 5448Δ*pmtA* mutant (see Fig. S7 in the supplemental material).

Under oxidative stress conditions, excess Fe(II) is capable of reacting with superoxide and $H_2O_2$ (10, 44). Fe-bound proteins may be vulnerable to damage by these reactive oxygen species, leading to the liberation of Fe as labile ions. If allowed to accumulate, this increased amount of Fe could further potentiate oxidative stress; thus, GAS possesses PmtA to efflux Fe(II) from the cell under oxidative stress conditions. As such, the 5448Δ*pmtA* deletion mutant, which contained higher levels of intracellular Fe(II) than did the WT strain, grew less efficiently in the presence of hydrogen peroxide and superoxide. Similarly, the *Salmonella enterica* serovar Typhimurium Fe efflux pump STM3944 mutant was shown to be more sensitive to hydrogen peroxide (45). The PerR regulon in GAS controls a variety of genes involved in the response to hydrogen peroxide stress (5). Here, we confirm that *pmtA* expression is upregulated by both Fe(II) and hydrogen peroxide and is regulated via PerR. The GAS ferritin-like protein Dpr (formerly MrgA) is also regulated by PerR (14) and has been shown to chelate Fe and protect GAS under conditions of oxidative stress (46). We hypothesize that GAS uses Dpr and PmtA to sequester and export Fe(II) under oxidative stress conditions, respec-

tively. Upon initial entry into the host, GAS undoubtedly encounters oxidative stress (23, 47). However, the lack of a virulence defect of the 5448Δ*pmtA* mutant in the mouse invasive disease model may reflect a niche-specific effect where this mutant is still able to survive and cause disease. Dpr may compensate for the loss of PmtA in the mouse model of invasive disease.

The necessity of maintaining the Fe/Mn ratio in Gram-positive bacteria such as *Streptococcus pneumoniae* and GAS is particularly important for defense against oxidative stress and pathogenesis (48–50). During oxidative stress, mismetallation of proteins can occur when the Fe/Mn ratio is disrupted (44). THY broth is a metal-rich microbiological medium; we have determined that THY broth as used in our laboratory contains approximately 15 $\mu$M Fe, which may explain the level of Fe accumulation that we observed in the 5448Δ*pmtA* mutant. Thus, when media and cells were treated with 2,2′-dipyridyl, the downregulation of *pmtA* may have been caused by a decreased amount of available Fe. Furthermore, the Mn rescue of the 5448Δ*pmtA* mutant when stressed with streptonigrin, Fe(II), and Co(II) is consistent with results obtained by examining PfeT of *B. subtilis* (18). We speculate that Fe might exert a toxic effect by mismetallating into Mn-containing metalloproteins. Thus, the addition of Mn relieves the toxic effect of excess Fe(II). In summary, PmtA represents an essential system for ensuring Fe(II) homeostasis in GAS, thus providing an important additional mechanism for resistance to oxidative stress.

## MATERIALS AND METHODS

**Phylogenetic and protein sequence analysis.** Sequences that share homology with *S. pyogenes* PmtA (see Table S1 in the supplemental material) were identified on the basis of a BLASTP search of the nonredundant GenBank database (NCBI) and included functionally characterized $P_{1B-4}$ ATPase amino acid sequences from *B. subtilis* PfeT (GenBank accession number CUB17201.1), *L. monocytogenes* FrvA (accession number NP_464168), and GAS PmtA (accession number AAZ51785.1). Determination of the P-type ATPase subclass was performed by using previously described methods (26). Protein sequences were aligned by using MUSCLE v3.8.31 (27) and trimmed to the common transmembrane domains 1 and 6 relative to the well-characterized PfeT protein from *Bacillus subtilis* (18). A best-fit phylogenetic tree was estimated by using RAxML v8.2.8 (51) based on the WAG substitution model with gamma correction of among-site rate variation. One hundred nonparametric bootstraps were applied.

**Bacterial strains and growth conditions.** The characterized invasive GAS M1T1 clinical strain 5448 was used in this study (31). 5448 WT and isogenic mutant strains were routinely cultured at 37°C in Todd-Hewitt broth (Difco) supplemented with 1% (wt/vol) yeast extract (Merck) (THY broth). For growth on solid medium, strains were cultured on 5% horse blood agar or THY agar (1.5%, wt/vol). *Escherichia coli* strains were grown in lysogeny broth (LB) (52). *E. coli* strain MC1061 was used for the maintenance of pHY304-derived plasmids, and the *E. coli* Top10 strain was used for the maintenance of pJRS233-derived plasmids (see Table S2 in the supplemental material). For the selection of GAS, the antibiotics kanamycin (300 $\mu$g/ml), spectinomycin (100 $\mu$g/ml), and erythromycin (2 $\mu$g/ml) were used. To select for *E. coli* plasmids, kanamycin (50 $\mu$g/ml), spectinomycin (100 $\mu$g/ml), and erythromycin (500 $\mu$g/ml) were used.

**DNA manipulations and mutant construction.** All GAS mutants were constructed according to standard operating procedures (50). Briefly, the construction of 5448Δ*pmtA* was achieved by the amplification of 5448 WT genomic DNA with primers pmtA-KO-1 (incorporating an XhoI site at the 5′ end) and pmtA-KO-2 (with homology to $Km^r$ at the 5′ end) to create the 5′-flanking region of *pmtA*. Primers pmtA-KO-3 (with homology to $Km^r$ at the 5′ end) and pmtA-KO-4 (incorporating a BamHI site at the 5′ end) were used to amplify the 3′-flanking region of *pmtA* (see Table S3 in the supplemental material). The $Km^r$ cassette was amplified from pUC4ΩKm2 by using primers km-F and km-R. The resultant fragments were amplified via 3-way PCR to form the construct pmtA-KO, which was ligated into the temperature-sensitive shuttle vector pHY304 to yield pHY304-pmtA-KO. The plasmid was electroporated into electrocompetent GAS cells as previously described (53). A double-crossover event was selected for, resulting in 5448Δ*pmtA*, which contains $Km^r$ (marker) and has lost $Ery^r$ (shuttle vector). Complementation of mutants was achieved by PCR amplification of the original *pmtA* allele using primers pmtA-KO-1 and pmtA-KO-4 and ligation into vector pJRS233, yielding pJRS233-pmtA, which was electroporated into 5448Δ*pmtA*. The plasmid was integrated via double crossover at 37°C for the replacement of $Km^r$ with *pmtA* at the original locus to yield 5448Δ*pmtA*::*pmtA*. All strains were confirmed by DNA sequencing conducted at the Australian Equine Genetics Research Centre at the University of Queensland.

**Growth analysis.** Growth analysis of 5448 WT, 5448Δ*pmtA*, and 5448Δ*pmtA*::*pmtA* was performed by using various amounts of $CoSO_4 \cdot 4H_2O$, $CuSO_4 \cdot 5H_2O$, $FeSO_4 \cdot 7H_2O$, $MnSO_4 \cdot 4H_2O$, $NiSO_4 \cdot 6H_2O$, $ZnSO_4 \cdot 7H_2O$, streptonigrin (Sigma), and methyl viologen (paraquat) (Sigma). All salts were analytical grade (Sigma). Metal solutions were prepared in deionized distilled water and filter sterilized. Streptonigrin was prepared with 100% ethanol and paraquat in deionized water. Cultures of GAS grown overnight in THY broth were diluted in fresh THY broth to an OD at 600 nm ($OD_{600}$) of 0.05 and supplemented with various

concentrations of the compound. The optical density was measured at 595 nm every 30 min while cells were grown statically at 37°C in a FLUOstar Optima plate reader (BMG Labtech) in flat-bottom 96-well plates (Greiner) (final volume of 200 μl/well). For growth in the presence of hydrogen peroxide, GAS strains 5448 WT, 5448Δ*pmtA*, and 5448Δ*pmtA*::*pmtA* were cultured at 37°C in THY broth or THY broth supplemented with 2 mM Fe(II). Bacteria were harvested at the mid-log growth phase and diluted to an $OD_{600}$ of 0.05 in THY broth with various concentrations of hydrogen peroxide, and the optical density at 595 nm was recorded. The doubling time was calculated by using the reciprocal of the gradient of natural-log-transformed $OD_{595}$ values during the exponential growth phase.

**Quantitative intracellular metal accumulation analysis.** Strains 5448 WT, 5448Δ*pmtA*, and 5448Δ*pmtA*::*pmtA* were grown to the mid-exponential growth phase ($OD_{600}$ = 0.6 to 0.8) in THY broth and challenged with an equal volume of either sterile deionized $H_2O$ or Fe(II) in $H_2O$ to a final concentration of 8 mM Fe(II), 1 mM Co(II), or 1 mM Zn(II) for 1 h at 37°C. Cells were harvested by centrifugation at 3,200 × *g* and washed 3 times with 1× phosphate-buffered saline (PBS) plus 250 mM EDTA and 3 times with 1× PBS, and a sample was taken to determine the total protein content by a bicinchoninic acid (BCA) assay (Thermo Scientific). Samples were digested in 70% nitric acid at 70°C for 48 h, diluted to 2% nitric acid, and analyzed by ICP-MS for Fe, Zn, and Co at the School of Geosciences at the University of Queensland. The metal content was normalized to the total protein content obtained from the BCA assay.

**RNA extraction.** Cultures of GAS grown overnight were diluted to an $OD_{600}$ of 0.025 in THY broth or THY medium supplemented with 8 mM Fe(II) or 50 μM 2,2′-dipyridyl. At the mid-exponential growth phase ($OD_{600}$ = 0.6 to 0.8), 5 ml of the culture was harvested by centrifugation at 8,000 × *g* for 10 min, and pellets were resuspended in TRIzol (Invitrogen), transferred to lysing matrix B tubes (MP Biomedicals), and mechanically lysed by using the FastPrep 120 instrument (Thermo Scientific). Alternatively, in experiments with 5448 WT, 5448Δ*perR*, and 5448Δ*perR*::*perR*, strains were grown to the mid-exponential phase and exposed to 5 mM $H_2O_2$ or 8 mM Fe(II) for 30 min, and the resultant bacterial pellets were processed identically. RNA was extracted from lysates by the addition of 0.2 volumes of chloroform, and phase separation of RNA was undertaken by centrifugation at 12,000 × *g* for 30 min at 4°C. The aqueous phase was removed, combined with 70% ethanol, and loaded onto RNeasy columns (Qiagen) for purification according to the manufacturer's recommendations. Following RNA elution in ultrapure water, RNA was DNase digested by using RNase-free DNase (Turbo; Ambion) according to the manufacturer's directions. RNA integrity was examined by gel electrophoresis and quantified by spectrophotometric analysis on the NanoDrop instrument (Thermo Scientific). PCR amplification of the RNA samples was performed to confirm the absence of genomic DNA contamination.

**Quantitative gene expression analysis.** A total of 500 ng of RNA was converted to cDNA by using Superscript III (Invitrogen) with random hexamers according to the manufacturer's directions. Quantitative PCR (qPCR) was performed by using SYBR green master mix (Applied Biosystems) with primer mixes at 100 nM and cDNA at 2 ng per reaction mixture on the Viia7 instrument (Applied Biosystems). qPCR primers used in this study are described in Table S3 in the supplemental material. Data were analyzed by using LinRegPCR (54) to obtain quantification cycle ($C_q$) values with *gyrA* as the reference gene, and data were plotted as $\Delta\Delta C_q$ values (55), using either THY broth alone or 5448 WT plus $H_2O$ as a control.

**Invasive model of GAS infection.** Transgenic humanized plasminogen mice heterozygous for the human plasminogen transgene (*AlbPLG1*$^{+/-}$) were infected with a dose of $2 \times 10^8$ to $4 \times 10^8$ CFU of 5448, 5448Δ*pmtA*, or 5448Δ*pmtA*::*pmtA*. Mice ($n$ = 10) were subcutaneously infected with freshly prepared GAS strains in 100 μl of 1× PBS, and virulence was assessed as previously described (56). All animal experiments were conducted according to the Guidelines for the Care and Use of Laboratory Animals (National Health and Medical Research Council, Australia) and were approved by the University of Queensland Animal Ethics Committee.

**Data analysis.** All data were analyzed by using GraphPad Prism 7. Analyses of ICP-MS and gene expression data were performed by using either 1-way analysis of variance (ANOVA) (for WT-only and single-condition experiments) or 2-way ANOVA (for comparison of strains under mixed conditions). Murine survival curves were analyzed by using the Mantel-Cox log rank test. Growth curve data represent means ± standard deviations of results from 3 independent biological replicates.

## SUPPLEMENTAL MATERIAL

Supplemental material for this article may be found at https://doi.org/10.1128/IAI.00140-17.

**SUPPLEMENTAL FILE 1,** PDF file, 1.3 MB.

## ACKNOWLEDGMENTS

A.G.T. is a recipient of the Australian Postgraduate Award. C.Y.O. is a recipient of a Garnett Passe & Rodney Williams Memorial Foundation research fellowship, and M.J.W. is an NHMRC Principal Research Fellow. This work was supported by the National Health and Medical Research Council (Australia).

We thank Matt Sweet for critically reading the manuscript.

A.G.T., C.Y.O., K.Y.D., A.G.M., and M.J.W. designed experiments. A.G.T. performed experimentation. M.R.D. performed phylogenetic analyses. N.P.W. provided reagents

and critiqued experimental design. A.G.T., C.Y.O., K.Y.D., M.R.D., A.G.M., and M.J.W. wrote the manuscript, and all authors edited the manuscript.

## REFERENCES


1. Brenot A, King KY, Janowiak B, Griffith O, Caparon MG. 2004. Contribution of glutathione peroxidase to the virulence of *Streptococcus pyogenes*. Infect Immun 72:408–413. https://doi.org/10.1128/IAI.72.1.408-413.2004.
2. King KY, Horenstein JA, Caparon MG. 2000. Aerotolerance and peroxide resistance in peroxidase and PerR mutants of *Streptococcus pyogenes*. J Bacteriol 182:5290–5299. https://doi.org/10.1128/JB.182.19.5290-5299.2000.
3. Lee JW, Helmann JD. 2006. The PerR transcription factor senses $H_2O_2$ by metal-catalysed histidine oxidation. Nature 440:363–367. https://doi.org/10.1038/nature04537.
4. Makthal N, Rastegari S, Sanson M, Ma Z, Olsen RJ, Helmann JD, Musser JM, Kumaraswami M. 2013. Crystal structure of peroxide stress regulator from *Streptococcus pyogenes* provides functional insights into the mechanism of oxidative stress sensing. J Biol Chem 288:18311–18324. https://doi.org/10.1074/jbc.M113.456590.
5. Brenot A, King KY, Caparon MG. 2005. The PerR regulon in peroxide resistance and virulence of *Streptococcus pyogenes*. Mol Microbiol 55:221–234. https://doi.org/10.1111/j.1365-2958.2004.04370.x.
6. Grifantini R, Toukoki C, Colaprico A, Gryllos I. 2011. Peroxide stimulon and role of PerR in group A *Streptococcus*. J Bacteriol 193:6539–6551. https://doi.org/10.1128/JB.05924-11.
7. Gerlach D, Reichardt W, Vettermann S. 1998. Extracellular superoxide dismutase from *Streptococcus pyogenes* type 12 strain is manganese-dependent. FEMS Microbiol Lett 160:217–224. https://doi.org/10.1111/j.1574-6968.1998.tb12914.x.
8. Toukoki C, Gryllos I. 2013. PolA1, a putative DNA polymerase I, is coexpressed with PerR and contributes to peroxide stress defenses of group A Streptococcus. J Bacteriol 195:717–725. https://doi.org/10.1128/JB.01847-12.
9. Reference deleted.
10. Anjem A, Imlay JA. 2012. Mononuclear iron enzymes are primary targets of hydrogen peroxide stress. J Biol Chem 287:15544–15556. https://doi.org/10.1074/jbc.M111.330365.
11. Imlay JA. 2003. Pathways of oxidative damage. Annu Rev Microbiol 57:395–418. https://doi.org/10.1146/annurev.micro.57.030502.090938.
12. Cornelis P, Wei Q, Andrews SC, Vinckx T. 2011. Iron homeostasis and management of oxidative stress response in bacteria. Metallomics 3:540–549. https://doi.org/10.1039/c1mt00022e.
13. Zhang TF, Ding Y, Li TT, Wan Y, Li W, Chen HC, Zhou R. 2012. A Fur-like protein PerR regulates two oxidative stress response related operons *dpr* and *metQIN* in *Streptococcus suis*. BMC Microbiol 12:85. https://doi.org/10.1186/1471-2180-12-85.
14. Tsou CC, Chiang-Ni C, Lin YS, Chuang WJ, Lin MT, Liu CC, Wu JJ. 2008. An iron-binding protein, Dpr, decreases hydrogen peroxide stress and protects Streptococcus pyogenes against multiple stresses. Infect Immun 76:4038–4045. https://doi.org/10.1128/IAI.00477-08.
15. Johnson MD, Kehl-Fie TE, Klein R, Kelly J, Burnham C, Mann B, Rosch JW. 2015. Role of copper efflux in pneumococcal pathogenesis and resistance to macrophage-mediated immune clearance. Infect Immun 83:1684–1694. https://doi.org/10.1128/IAI.03015-14.
16. Young CA, Gordon LD, Fang Z, Holder RC, Reid SD. 2015. Copper tolerance and the characterization of a copper-responsive operon, *copYAZ*, in an M1T1 clinical strain of *Streptococcus pyogenes*. J Bacteriol 197:2580–2592. https://doi.org/10.1128/JB.00127-15.
17. Fu Y, Tsui HC, Bruce KE, Sham LT, Higgins KA, Lisher JP, Kazmierczak KM, Maroney MJ, Dann CE, III, Winkler ME, Giedroc DP. 2013. A new structural paradigm in copper resistance in Streptococcus pneumoniae. Nat Chem Biol 9:177–183. https://doi.org/10.1038/nchembio.1168.
18. Guan G, Pinochet-Barros A, Gaballa A, Patel SJ, Arguello JM, Helmann JD. 2015. PfeT, a P1B4-type ATPase, effluxes ferrous iron and protects *Bacillus subtilis* against iron intoxication. Mol Microbiol 98:787–803. https://doi.org/10.1111/mmi.13158.
19. Pi H, Patel SJ, Arguello JM, Helmann JD. 2016. The *Listeria monocytogenes* Fur-regulated virulence protein FrvA is an Fe(II) efflux P-type ATPase. Mol Microbiol 100:1066–1079. https://doi.org/10.1111/mmi.13368.
20. Carapetis JR, Steer AC, Mulholland EK, Weber M. 2005. The global burden of group A streptococcal diseases. Lancet Infect Dis 5:685–694. https://doi.org/10.1016/S1473-3099(05)70267-X.
21. Walker MJ, Barnett TC, McArthur JD, Cole JN, Gillen CM, Henningham A, Sriprakash KS, Sanderson-Smith ML, Nizet V. 2014. Disease manifestations and pathogenic mechanisms of group A *Streptococcus*. Clin Microbiol Rev 27:264–301. https://doi.org/10.1128/CMR.00101-13.
22. Cole JN, Barnett TC, Nizet V, Walker MJ. 2011. Molecular insight into invasive group A streptococcal disease. Nat Rev Microbiol 9:724–736. https://doi.org/10.1038/nrmicro2648.
23. Henningham A, Dohrmann S, Nizet V, Cole JN. 2015. Mechanisms of group A *Streptococcus* resistance to reactive oxygen species. FEMS Microbiol Rev 39:488–508. https://doi.org/10.1093/femsre/fuu009.
24. Sumby P, Porcella SF, Madrigal AG, Barbian KD, Virtaneva K, Ricklefs SM, Sturdevant DE, Graham MR, Vuopio-Varkila J, Hoe NP, Musser JM. 2005. Evolutionary origin and emergence of a highly successful clone of serotype M1 group A *Streptococcus* involved multiple horizontal gene transfer events. J Infect Dis 192:771–782. https://doi.org/10.1086/432514.
25. Brenot A, Weston BF, Caparon MG. 2007. A PerR-regulated metal transporter (PmtA) is an interface between oxidative stress and metal homeostasis in *Streptococcus pyogenes*. Mol Microbiol 63:1185–1196. https://doi.org/10.1111/j.1365-2958.2006.05577.x.
26. Smith AT, Smith KP, Rosenzweig AC. 2014. Diversity of the metal-transporting P1B-type ATPases. J Biol Inorg Chem 19:947–960. https://doi.org/10.1007/s00775-014-1129-2.
27. Edgar RC. 2004. MUSCLE: multiple sequence alignment with high accuracy and high throughput. Nucleic Acids Res 32:1792–1797. https://doi.org/10.1093/nar/gkh340.
28. Krogh A, Larsson B, von Heijne G, Sonnhammer ELL. 2001. Predicting transmembrane protein topology with a hidden Markov model: application to complete genomes. J Mol Biol 305:567–580. https://doi.org/10.1006/jmbi.2000.4315.
29. Argüello JM. 2003. Identification of ion-selectivity determinants in heavy-metal transport P1B-type ATPases. J Membr Biol 195:93–108. https://doi.org/10.1007/s00232-003-2048-2.
30. Argüello JM, González-Guerrero M, Raimunda D. 2011. Bacterial transition metal P1B-ATPases: transport mechanism and roles in virulence. Biochemistry 50:9940–9949. https://doi.org/10.1021/bi201418k.
31. Chatellier S, Ihendyane N, Kansal RG, Khambaty F, Basma H, Norrby-Teglund A, Low DE, McGeer A, Kotb M. 2000. Genetic relatedness and superantigen expression in group A *Streptococcus* serotype M1 isolates from patients with severe and nonsevere invasive diseases. Infect Immun 68:3523–3534. https://doi.org/10.1128/IAI.68.6.3523-3534.2000.
32. Yeowell HN, White JR. 1982. Iron requirement in the bactericidal mechanism of streptonigrin. Antimicrob Agents Chemother 22:961–968. https://doi.org/10.1128/AAC.22.6.961.
33. Gryllos I, Grifantini R, Colaprico A, Cary ME, Hakansson A, Carey DW, Suarez-Chavez M, Kalish LA, Mitchell PD, White GL, Wessels MR. 2008. PerR confers phagocytic killing resistance and allows pharyngeal colonization by group A *Streptococcus*. PLoS Pathog 4:e1000145. https://doi.org/10.1371/journal.ppat.1000145.
34. Ricci S, Janulczyk R, Bjorck L. 2002. The regulator PerR is involved in oxidative stress response and iron homeostasis and is necessary for full virulence of *Streptococcus pyogenes*. Infect Immun 70:4968–4976. https://doi.org/10.1128/IAI.70.9.4968-4976.2002.
35. Skaar EP. 2010. The battle for iron between bacterial pathogens and their vertebrate hosts. PLoS Pathog 6:e1000949. https://doi.org/10.1371/journal.ppat.1000949.
36. Montanez GE, Neely MN, Eichenbaum Z. 2005. The streptococcal iron uptake (Siu) transporter is required for iron uptake and virulence in a zebrafish infection model. Microbiology 151:3749–3757. https://doi.org/10.1099/mic.0.28075-0.
37. Francis RT, Jr, Booth JW, Becker RR. 1985. Uptake of iron from hemoglobin and the haptoglobin-hemoglobin complex by hemolytic bacteria. Int J Biochem 17:767–773. https://doi.org/10.1016/0020-711X(85)90262-9.

38. Eichenbaum Z, Muller E, Morse SA, Scott JR. 1996. Acquisition of iron from host proteins by the group A *Streptococcus*. Infect Immun 64:5428–5429.
39. Nygaard TK, Blouin GC, Liu M, Fukumura M, Olson JS, Fabian M, Dooley DM, Lei B. 2006. The mechanism of direct heme transfer from the streptococcal cell surface protein Shp to HtsA of the HtsABC transporter. J Biol Chem 281:20761–20771. https://doi.org/10.1074/jbc.M601832200.
40. Hanks TS, Liu M, McClure MJ, Lei B. 2005. ABC transporter FtsABCD of *Streptococcus pyogenes* mediates uptake of ferric ferrichrome. BMC Microbiol 5:62. https://doi.org/10.1186/1471-2180-5-62.
41. Smith JL. 2004. The physiological role of ferritin-like compounds in bacteria. Crit Rev Microbiol 30:173–185. https://doi.org/10.1080/10408410490435151.
42. Frawley ER, Fang FC. 2014. The ins and outs of bacterial iron metabolism. Mol Microbiol 93:609–616. https://doi.org/10.1111/mmi.12709.
43. Munkelt D, Grass G, Nies DH. 2004. The chromosomally encoded cation diffusion facilitator proteins DmeF and FieF from *Wautersia metallidurans* CH34 are transporters of broad metal specificity. J Bacteriol 186:8036–8043. https://doi.org/10.1128/JB.186.23.8036-8043.2004.
44. Sobota JM, Imlay JA. 2011. Iron enzyme ribulose-5-phosphate 3-epimerase in *Escherichia coli* is rapidly damaged by hydrogen peroxide but can be protected by manganese. Proc Natl Acad Sci U S A 108:5402–5407. https://doi.org/10.1073/pnas.1100410108.
45. Frawley ER, Crouch ML, Bingham-Ramos LK, Robbins HF, Wang W, Wright GD, Fang FC. 2013. Iron and citrate export by a major facilitator superfamily pump regulates metabolism and stress resistance in *Salmonella* Typhimurium. Proc Natl Acad Sci U S A 110:12054–12059. https://doi.org/10.1073/pnas.1218274110.
46. Tsou CC, Chiang-Ni C, Lin YS, Chuang WJ, Lin MT, Liu CC, Wu JJ. 2010. Oxidative stress and metal ions regulate a ferritin-like gene, *dpr*, in *Streptococcus pyogenes*. Int J Med Microbiol 300:259–264. https://doi.org/10.1016/j.ijmm.2009.09.002.
47. Babior BM. 2000. Phagocytes and oxidative stress. Am J Med 109:33–44. https://doi.org/10.1016/S0002-9343(00)00481-2.
48. Ong CLY, Potter AJ, Trappetti C, Walker MJ, Jennings MP, Paton JC, McEwan AG. 2013. Interplay between manganese and iron in pneumococcal pathogenesis: role of the orphan response regulator RitR. Infect Immun 81:421–429. https://doi.org/10.1128/IAI.00805-12.
49. Rosch JW, Gao G, Ridout G, Wang YD, Tuomanen EI. 2009. Role of the manganese efflux system MntE for signalling and pathogenesis in *Streptococcus pneumoniae*. Mol Microbiol 72:12–25. https://doi.org/10.1111/j.1365-2958.2009.06638.x.
50. Turner AG, Ong CL, Gillen CM, Davies MR, West NP, McEwan AG, Walker MJ. 2015. Manganese homeostasis in group A Streptococcus is critical for resistance to oxidative stress and virulence. mBio 6:e00278–15. https://doi.org/10.1128/mBio.00278-15.
51. Stamatakis A. 2014. RAxML version 8: a tool for phylogenetic analysis and post-analysis of large phylogenies. Bioinformatics 30:1312–1313. https://doi.org/10.1093/bioinformatics/btu033.
52. Bertani G. 1951. Studies on lysogenesis. I. The mode of phage liberation by lysogenic *Escherichia coli*. J Bacteriol 62:293–300.
53. Venturini C, Ong CY, Gillen CM, Ben-Zakour NL, Maamary PG, Nizet V, Beatson SA, Walker MJ. 2013. Acquisition of the Sda1-encoding bacteriophage does not enhance virulence of the serotype M1 *Streptococcus pyogenes* strain SF370. Infect Immun 81:2062–2069. https://doi.org/10.1128/IAI.00192-13.
54. Ramakers C, Ruijter JM, Deprez RH, Moorman AF. 2003. Assumption-free analysis of quantitative real-time polymerase chain reaction (PCR) data. Neurosci Lett 339:62–66. https://doi.org/10.1016/S0304-3940(02)01423-4.
55. Livak KJ, Schmittgen TD. 2001. Analysis of relative gene expression data using real-time quantitative PCR and the $2^{-\Delta\Delta}$ method. Methods 25:402–408. https://doi.org/10.1006/meth.2001.1262.
56. Walker MJ, Hollands A, Sanderson-Smith ML, Cole JN, Kirk JK, Henningham A, McArthur JD, Dinkla K, Aziz RK, Kansal RG, Simpson AJ, Buchanan JT, Chhatwal GS, Kotb M, Nizet V. 2007. DNase Sda1 provides selection pressure for a switch to invasive group A streptococcal infection. Nat Med 13:981–985. https://doi.org/10.1038/nm1612.